Supplement 1:
Translation of Section 5.7 of GSK (2019) on 'Earthquake magnitude determination'

This supplement provides a paraphrased translation of Section 5.7 of GSK (2019). A direct translation revealed the original text to be rather long-winded, with extraneous digressions (e.g., regarding whether earthquake magnitudes should be expressed to one or two decimal places) and several obscurities and inconsistencies. In the following translation, unnecessary verbosity has been removed; some inconsistencies and obscurities remain although others have been eliminated where possible using information from other sources, the latter points being enclosed in brackets.

Of the total of 520 earthquakes identified in the vicinity of the Pohang EGS project [between latitudes 35.552 and 36.618°N and longitudes 128.988 and 129.935°E] between February 2009 and the Pohang mainshock on 15 November 2017 (listed in Appendix A-6, tab GSK_A-6 of Supplement 3), magnitudes could be determined for 137 events. For this study, preliminary values of local magnitude (M_L) were determined using the vertical component equation of Sheen et al. (2018), which predicts magnitude as a function of the maximum amplitude of seismic phases and source-station distance. [The maximum amplitude used in this process is that determined for synthetic Wood-Anderson seismograms, as described by Sheen et al. (2018), not for the raw seismograms.] However, due to different site characteristics, the data from individual seismograph stations show M_L variations of 0.54 for horizontal component data and 0.29 for vertical component data. More reliable magnitude determinations therefore require correction for the seismograph stations used. Station corrections were therefore determined using data for aftershocks between 16 November and 31 December 2017.

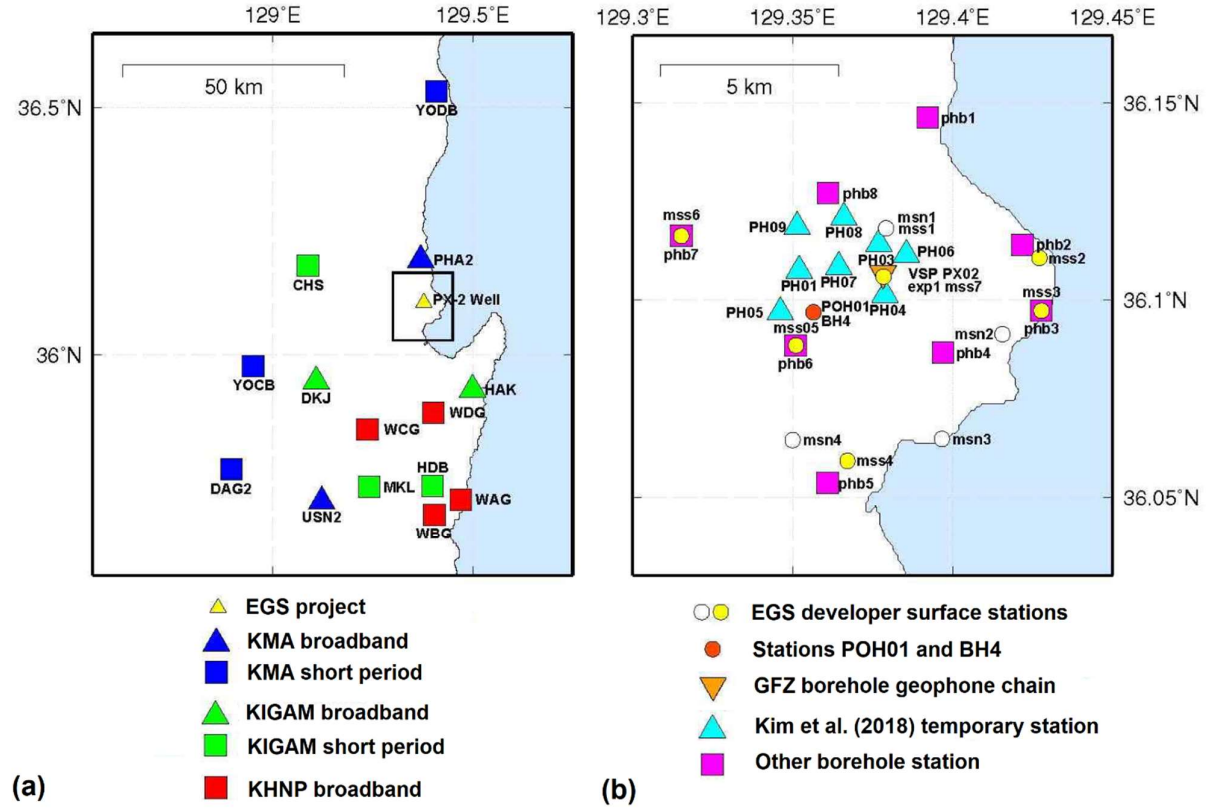

Figure S1-1 (from Fig. 5-1). (a) Map of seismograph stations used in this study. (a) Permanent regional network consisting of stations operated by the Korea Meteorological Administration (KMA), the Korea Institute of Geoscience and Mineral Resources (KIGAM), and Korea Hydro & Nuclear Power (KHNP). The KHNP network monitors seismicity near the Wolseong complex of nuclear power plants to the south of Pohang. (b) Temporary stations installed in the vicinity of the EGS site by the EGS developer, their collaborators, and others.

[At this time, seismograph stations were operational in the Pohang area from multiple networks (Fig. S1-1), including the permanent networks of the Korea Meteorological Administration (KMA) and the Korea Institute of Geoscience and Mineral Resources (KIGAM), the temporary network for the EGS project, and other temporary stations for monitoring aftershocks of the 15 November 2017 earthquake.] A catalogue of 194 earthquakes [between 16 November and 31 December 2017] was compiled, each with ≥5 seismic arrivals observed by the KMA and KIGAM networks. An initial 'network magnitude' M_N was determined, after Sheen et al. (2018), for each of these events, averaged across the stations that reported the event. The differences between M_N and the corresponding magnitude for each station were then averaged to determine the magnitude correction ΔM_L for each station. For stations with multiple instruments, such as broadband seismometers and accelerometers, ΔM_L was determined separately for each type of instrument.

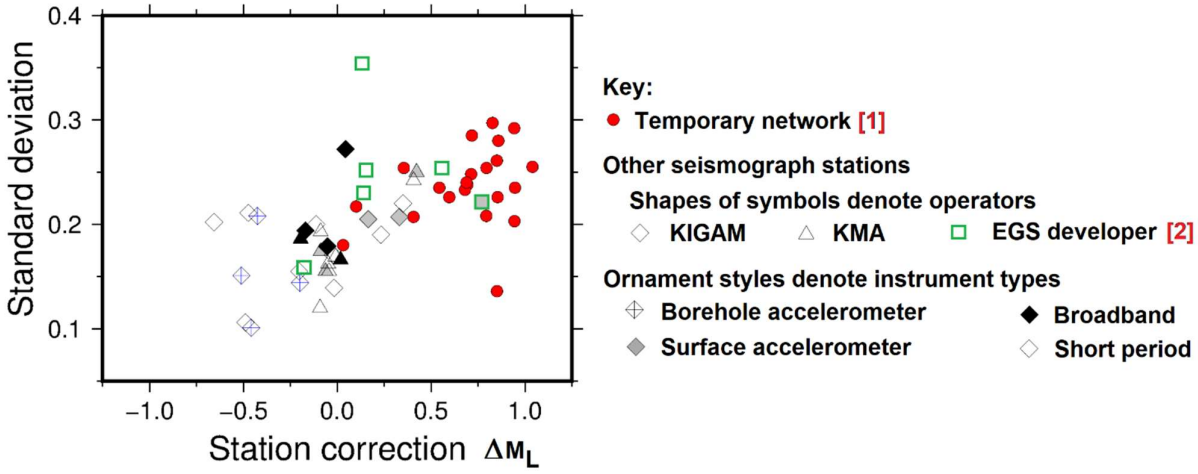

Figure S1-2 (from Fig. 5-7). Comparison of the station corrections for DM_L, the difference between local magnitude M_L as measured for each station and the 'network magnitude' M_N as defined in the text, for a set of 194 earthquakes between 16 November and 31 December 2017. For each station that yielded data, the mean 'station correction' is plotted on the horizontal axis and the associated standard deviation on the vertical axis. This diagram shows that the KMA and KIGAM stations yield M_L values that do not depart systematically from M_N, but the 'EGS developer' and 'temporary network' stations yield M_L values that typically exceed M_N by large margins. Notes: [1] the wording appears to indicate that the 'temporary network' stations are those listed as 'Kim et al. (2018) temporary stations' and 'other borehole stations' in Fig. S1-1. However, it is unclear why 16 stations in these networks are shown in Fig. S1-1 but 22 symbols are depicted here; [2] The 'EGS developer' stations include those of the network operated on behalf of the developer, NexGeo, by KIGAM, plus the additional stations provided by GFZ Potsdam and ETH Zürich as part of collaborations.

The resulting magnitude corrections, determined for 44 seismometers [using this set of 194 earthquakes between 16 November and 31 December 2017], are shown in Fig. S1-2. For the broadband instruments, ΔM_L ranges from -0.170 to 0.044 for the KIGAM stations and from -0.195 to 0.180 for the KMA stations. For the short period seismometers, ΔM_L ranges from 0.165 to 0.331 for the KIGAM stations and from -0.089 to 0.422 for the KMA stations. For the accelerometers, ΔM_L ranges from -0.657 to 0.350 for the KIGAM stations and from -0.092 to 0.406 for the KMA stations. Where two types of instrument were installed in the same place, the ΔM_L values typically differ by only 0.014 ± 0.083 (i.e., they are very similar to each other). In contrast, ΔM_L ranges from -0.179 to 0.768 for the instruments operated on behalf of the EGS developer and from 0.031 to 1.286 for the temporary network to monitor aftershocks of the 15 November 2017 earthquake. [As Fig. 5-7 indicates, for each earthquake the magnitudes determined using stations of these latter two networks are thus, typically, rather higher than the value of M_N determined using the instruments of the permanent networks in the area. Furthermore, the source parameters for this set of 194 earthquakes were not reported by GSK (2019).]

Using the Sheen et al. (2018) formula, with this set of ΔM_L station corrections, M_L has been determined for 40 earthquakes between 30 November 2015 and 15 November 2017. The resulting M_L values range from 0.15 to 5.33, with a typical standard deviation of ±0.14. In addition, M_L 2.16 was determined for an earthquake, ~12 km below the EGS site, at 08:06 on 1 March 2013. For the 15 November 2017 mainshock,

M_L 5.33±0.14 was determined using records from 11 broadband seismometers, short period seismometers, and accelerometers within ~50 km of the site; M_L 5.34±0.18 was determined using 77 broadband seismometers installed throughout the Korean Peninsula, in close agreement.

The M_L scale, as defined by Richter (1935), is based on the maximum amplitude of seismograms recorded by Wood-Anderson seismographs, the response of which amplifies a band of low frequencies. This response can be simulated for records from modern digital seismometers, but when this was attempted it was found that the maximum amplitude of many resulting records could not be reliably measured, making M_L determination by this method [(i.e., by the Sheen et al. (2018) procedure).] impossible.

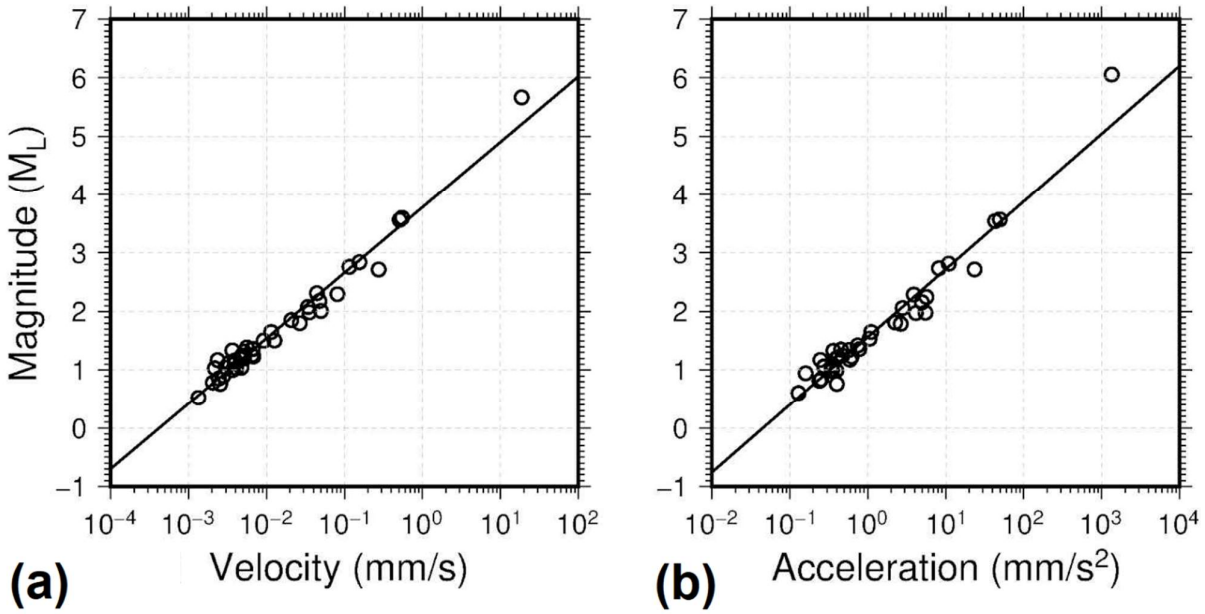

Figure S1-3 (from Fig. 5-8). Plots of peak velocity V_M (a) and peak acceleration A_M (b) recorded on the seismometers and accelerometers at KMA station PHA2 against magnitude M_L for the 40 earthquakes for which M_L could be determined independently. These values are fitted with straight lines that define empirical prediction equations for the prediction of M_L from V_M or A_M for other earthquakes, subject to the assumption of the same hypocentral distance. The prediction equations thus defined are: $M_L = 3.765 + 1.117 \log_{10}(V_M / \text{mm s}^{-1})$ and $M_L = 1.576 + 1.152 \log_{10}(A_M / \text{mm s}^{-2})$.

To estimate M_L for other earthquakes, the maximum amplitudes of the short period seismometer and accelerometer data from KMA station PHA2 (~10 km north of the EGS site; Fig. S1-1), for the 40 earthquakes that established the station corrections to define the M_L scale, were used to derive prediction equations for M_L (Fig. S1-3). The maximum amplitudes used were measured from the seismograms and accelerograms without removing their instrumental response and without integration to obtain records of ground displacement. M_L values for 72 earthquakes that have been located were thus determined. Seismic phases from many other earthquakes have also been identified using template matching, but are insufficient for location. For 24 of these small earthquakes, maximum amplitudes could be measured at station PHA2, from which M_L was determined using these prediction equations, with estimated uncertainties circa ±0.2. [Overall, using this combination of methods, M_L has been determined for 137 events: the 40 'calibration' events during 2015-2017, the event of 2013, and the 96 events for which the prediction equations were used. However, the reporting by GSK (2019) does not indicate which of the M_L values were determined by which method.]

Moment magnitudes (M_W) were also determined for 48 of the aforementioned 137 earthquakes [In fact, Table 5-6 of GSK (2019) shows that M_W was determined for 50 of these 137 events]. To this end, the near-source rock density and P-wave velocity were assumed to be 2800 kg m^{-3} and 6 km s^{-1}. For most events, M_W was determined in the time domain after Tsuboi et al. (1995) and Prejean and Ellsworth (2001). Seismic moment was thus measured (after Aki and Richards, 1980) from the area of the initial P-wave displacement waveform observed at station PHA2, to give M_W for 46 earthquakes. M_W was also determined for the

15 November 2017 mainshock using its P-wave displacement spectrum, after Rhee and Sheen (2016). Spectra were derived from velocity seismograms, each sampled over a 20.48 s time window, from 58 broadband stations at distances of ≥150 km where the P- and S-waves were sufficiently distinguished. P-wave spectra were corrected for anelastic attenuation after Kim et al. (2006). Using the Brune (1970) seismic source model, seismic moment was determined, giving M_W 5.56±0.18, with P-wave corner frequency 0.60 Hz, stress drop 5.6 MPa, and source radius 3.44 km.

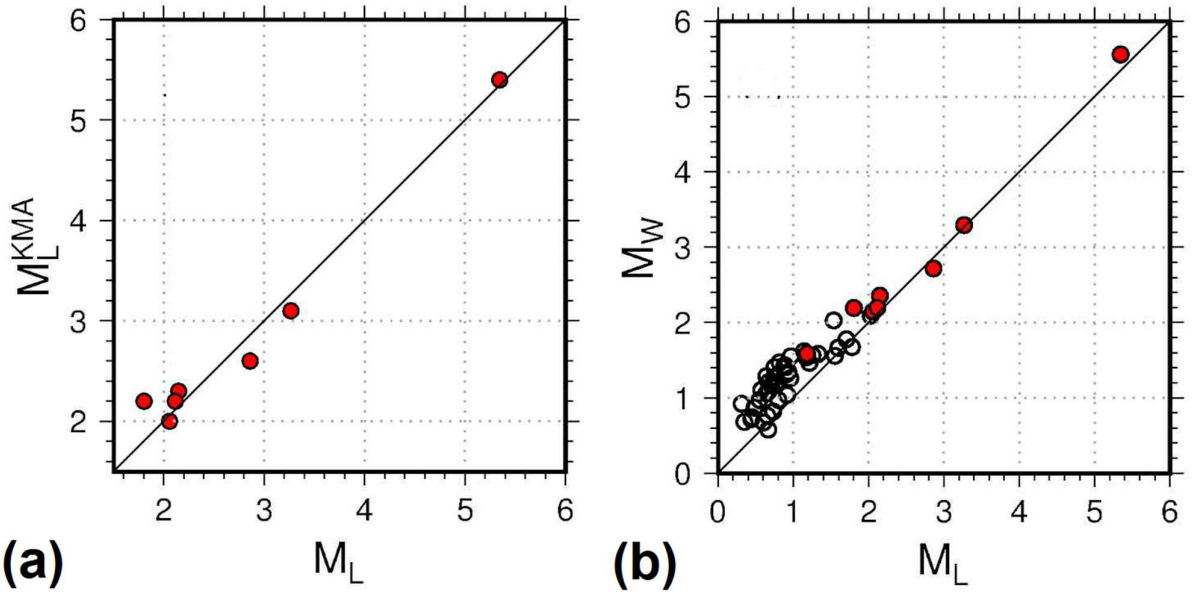

Figure S1-4 (from Fig. 5-9). Comparison of magnitude estimates. (a) Comparison of KMA local magnitudes with M_L values determined in this study, for the seven events for which KMA reported magnitudes and published source parameters. (b) Comparison of M_W and M_L values, as determined in the present study, for the 46 events for which both were determined, including the seven events depicted in (a), which are highlighted.

[Appendix A-5 lists source parameters derived in this study for 98 earthquakes, spanning November 2015 to the time of the 15 November 2017 mainshock, with epicentres between 36.1037 and 36.1146°N and between 129.3691 and 129.3781°E (i.e., within ~0.5 km of the EGS site). M_L has been determined for all these events, the smallest having M_L -0.77, and M_W for 46 of them, the smallest with M_W 0.58 and M_L 0.67, M_W 0.72 and M_L 0.44, M_W 0.74 and M_L 0.45, M_W 0.76 and M_L 0.66, M_W 0.82 and M_L 0.73, M_W 0.87 and M_L 0.48, M_W 0.92 and M_L 0.31, whereas KMA determined their own M_L≥2.0 for 7 of these events.] Figure S1-4 compares these magnitude determinations, illustrating strong correlations. The results for the mainshock (M_L=5.35; M_W=5.56) are also consistent with the independent determinations of M_W 5.5 by Grigoli et al. (2018) and 5.4 by Kim et al. (2018).

During several recent EGS projects, b-values ranged from a high of 1.58 at Basel, Switzerland (Bachmann et al., 2011), between 0.9 and 1.2 at Soultz-sous-Forêts, France (Dorbath et al., 2009), and a low of 0.83 in the Cooper Basin, Australia (Baisch et al., 2009). For the five Pohang stimulations a b-value of 0.73±0.1 is observed (Fig. S1-5). This relatively low b-value corresponds to a higher likelihood of a large magnitude event compared to either the other EGS projects or to global tectonic seismicity generally. It should be noted that the low b-values in the Cooper Basin and the lowest at Soultz-sous-Forêts corresponded to stimulations that activated discrete faults, whereas the high b-value stimulation at Basel activated a volume.

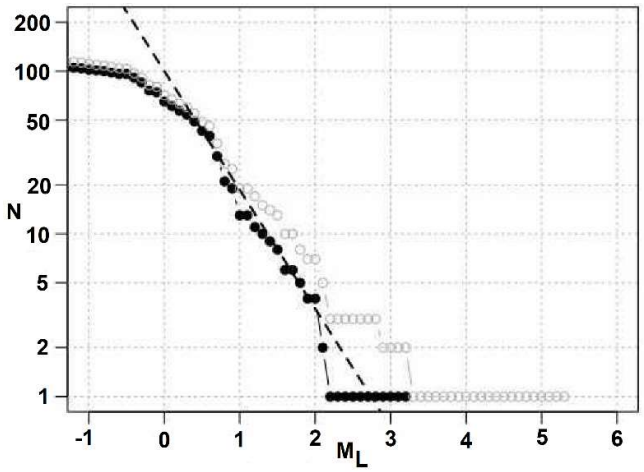

Figure S1-5 (from Fig. O-12). Gutenberg-Richter magnitude-frequency diagram. Solid symbols denote earthquakes during or after the five Pohang stimulations. The dashed line, determined after of Tinti and Mulargia (1985), has the equation $\log_{10}(N) = 2.0 - 0.73\ M_L$. Open symbols include foreshocks, mainshock and stimulation events.

References

Aki, K., Richards, P.G., 1980. Quantitative Seismology: Theory and Methods. Freeman, San Francisco, 913 pp.

Bachmann, C. E., Wiemer, S., Woessner, J., Hainzl, S., 2011. Statistical analysis of the induced Basel 2006 earthquake sequence: Introducing a probability-based monitoring approach for Enhanced Geothermal Systems. *Geophysical Journal International*, **186**, 793-807.

Baisch, S., Vörös, R., Weidler, R., Wyborn, D., 2009. Investigation of fault mechanisms during geothermal reservoir stimulation experiments in the Cooper Basin, Australia. *Bulletin of the Seismological Society of America*, **99**, 148-158.

Brune, J.N., 1970. Tectonic stress and the spectra of seismic shear waves from earthquakes. *Journal of Geophysical Research*, **75**, 4997-5009.

Dorbath, L., Cuenot, N., Genter, A., Frogneux, M., 2009. Seismic response of the fractured and faulted granite of Soultz-sous-Forêts (France) to 5 km deep massive water injections. *Geophysical Journal International*, **177**, 653-675.

Grigoli, F., Cesca, S., Rinaldi, A.P., Manconi, A., Lopez-Comino, J.A., Clinton, J.F., Westaway, R., Cauzzi, C., Dahm, T., Wiemer, S., 2018. The November 15, 2017 Pohang earthquake: A probable induced event of M_W 5.5 in South Korea. *Science*, **360**, 1003-1006.

Kim, K.-H., Ree, J.-H., Kim, Y., Kim, S., Kang, S.Y., Seo, W., 2018, Assessing whether the 2017 M_W 5.4 Pohang earthquake in South Korea was an induced event. *Science*, **360**, 1007-1009.

Kim, S. K., Yang, J. Y., Oh, J., 2006. Q-values for P and S waves in the southern Korean peninsula based on the coda-normalization method. *Geosciences Journal*, **10**, 465-477.

Prejean, S.G., Ellsworth, W.L., 2001. Observations of earthquake source parameters at 2 km depth in the Long Valley Caldera, eastern California. *Bulletin of the Seismological Society of America*, **91**, 165-177.

Richter, C.F., 1935. An instrumental earthquake magnitude scale. *Bulletin of the Seismological Society of America*, **25**, 1-32.

Rhee, H.-M., Sheen, D.-H., 2016. Lateral variation in the source parameters of earthquakes in the Korean Peninsula. *Bulletin of the Seismological Society of America*, **106**, 2266-2274.

Sheen, D.-H, Kang, T.-S., Rhie, J., 2018. A local magnitude scale for South Korea. *Bulletin of the Seismological Society of America*, **108**, 2748-2755.

Tinti, S., Mulargia, F., 1985. Effects of magnitude uncertainties on estimating the parameters in the Gutenberg-Richter frequency-magnitude law. *Bulletin of the Seismological Society of America*, **75**, 1681-1697.

Tsuboi, K., Abe, K., Takano, K., Yamanaka, Y., 1995. Rapid determination of M_W from broadband P waveforms. *Bulletin of the Seismological Society of America*, **85**, 606-613.

Supplement 2:
Instrumental frequency responses

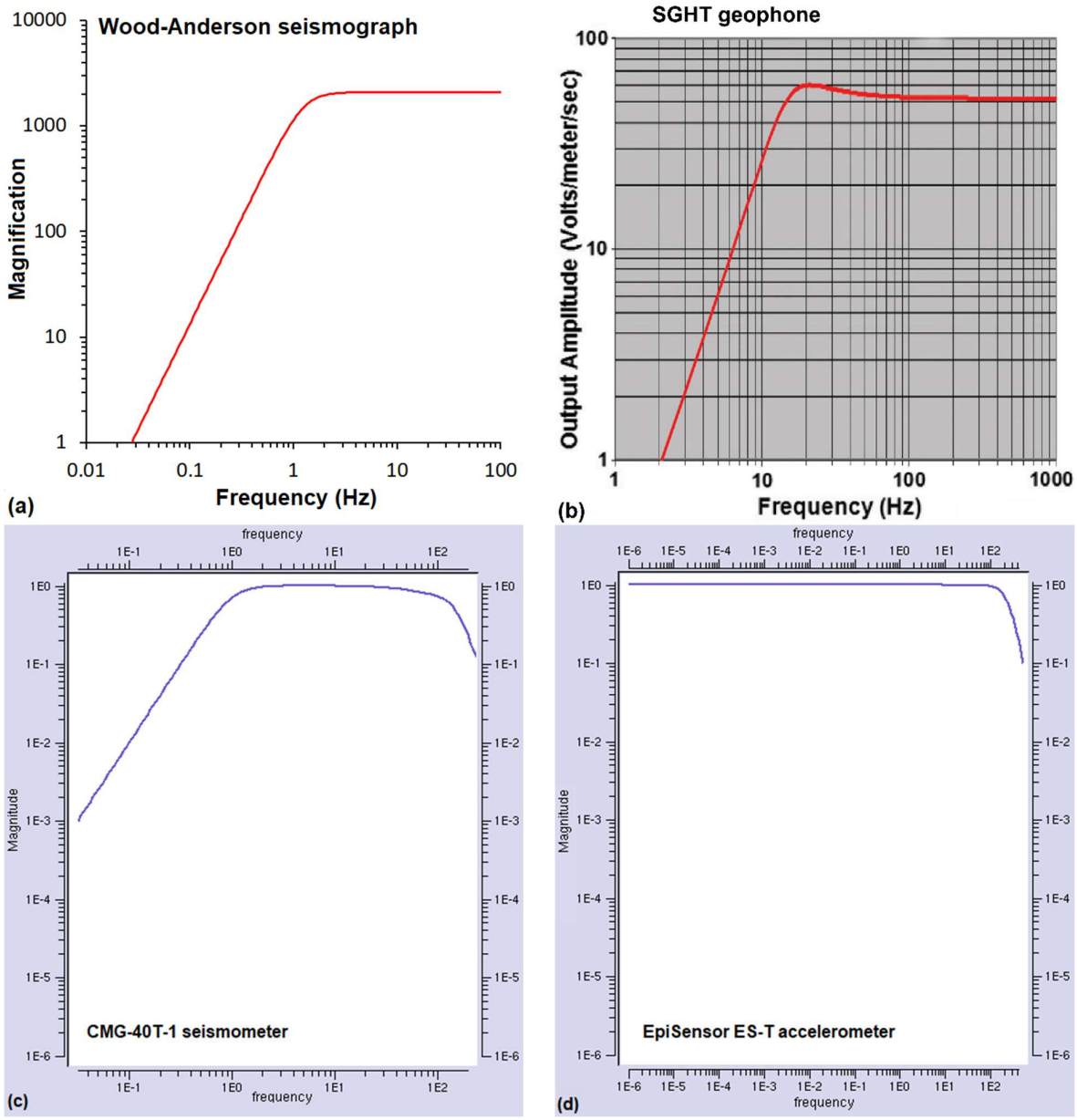

Figure S2-1. Amplitude responses of instruments relevant to earthquake monitoring at Pohang. **(a)** Response of a standard Wood-Anderson seismograph, with a natural period 0.8 s (natural frequency 1.25 Hz), from Fig. 1 of Uhrhammer and Collins (1990). This response characteristic indicates how the amplitude of the seismogram trace relates to ground velocity. **(b)** Instrumental response of a Sercel SGHT-15 geophone with natural frequency 15 Hz, as used in the GFZ geophone chain, to frequencies of ground velocity. From Sercel (2019). **(c)** Instrumental response of a Güralp CMG-40T-1 seismometer, flat between frequencies of 1 and 100 Hz, as used at stations PHA2 and MSS01, to frequencies of ground velocity. From IRIS PASSCAL (2020a). **(d)** Instrumental response of a Kinemetrics EpiSensor ES-T accelerometer, flat to 200 Hz, as used at station PHA2, to frequencies of ground acceleration. From IRIS PASSCAL (2020b).

Figure S2-1 illustrates the amplitude responses as a function of frequency of seismic sensors relevant to the Pohang case study. The cited reference sources also provide the corresponding phase responses. These include the Wood-Anderson seismometer, synthesis of which is required for Richter's (1935) definition of M_L, the Sercel SGHT-15 geophone, used in the geophone chain deployed in Pohang well PX-2 by Geoforschungs Zentrum Potsdam during the August 2017 stimulation of well PX-1 (Hofmann et al., 2019), and the Güralp CMG-40T-1

seismometer and Kinemetrics EpiSensor ES-T accelerometer, installed at KMA station PHA2 and providing data used in the analyses by GSK (2019), Woo et al. (2019), and Langenbruch et al. (2020). Figure S2-2 illustrates the amplitude response of the Trillium Compact broadband sensor. The analysis by Kwiatek and Ben-Zion (2016), illustrating the effect of frequency truncation of recording on magnitude determination, was for the variant with natural period 120 s.

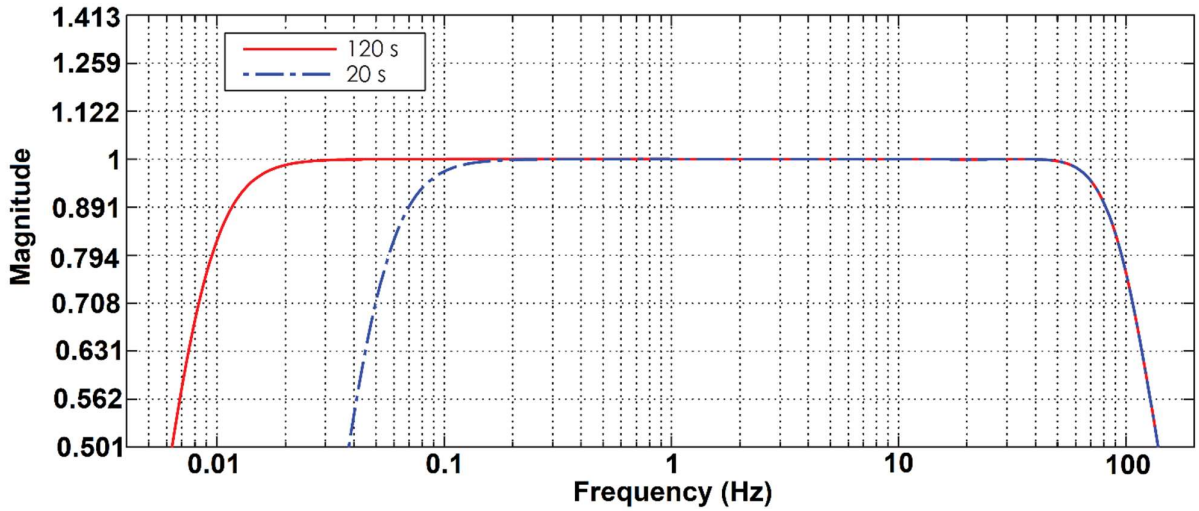

Figure S2-2. Amplitude response of the Trillium Compact sensor, from Nanometrics (2015).

References

GSK, 2019. Final Report of the Korean Government Commission on relations between the 2017 Pohang Earthquake and EGS Project. The Geological Society of Korea, Seoul, 427 pp. (in Korean). https://data.doi.or.kr/10.22719/KETEP-2019043001

Hofmann, H., Zimmermann, G., Farkas, M., Huenges, E., Zang, A., Leonhardt, M., Kwiatek, G., Martinez-Garzon, P., Bohnhoff, M., Min, K.-B., Fokker, P., Westaway, R., Bethmann, F., Meier, P., Yoon, K.S., Choi, J.W., Lee, T.J., Kim, K.Y., 2019. First field application of cyclic soft stimulation at the Pohang Enhanced Geothermal System site in Korea. *Geophysical Journal International*, **217**, 926–949.

IRIS PASSCAL, 2020a. Guralp CMG-40T-1 Short period sensor. IRIS PASSCAL Instrument Center, Socorro, New Mexico. https://www.passcal.nmt.edu/content/instrumentation/sensors/short-period-sensors/cmg-40t-1-sp-sensor

IRIS PASSCAL, 2020b. Kinemetrics Episensor ES-T accelerometer. IRIS PASSCAL Instrument Center, Socorro, New Mexico. https://www.passcal.nmt.edu/content/instrumentation/sensors/accelerometers/kinemetrics-accelerometer

Kwiatek, G., Ben-Zion, Y., 2016. Theoretical limits on the detection and analysis of small earthquakes. *Journal of Geophysical Research, Solid Earth*, **121**, 5898–5916. https://doi.org/10.1002/2016JB012908.

Langenbruch, C., Ellsworth, W.L., Woo, J.-U., Wald, D.J., 2020. Value at induced risk: injection-induced seismic risk from low-probability, high-impact events. *Geophysical Research Letters*, **47**, e2019GL085878, 12 pp., https://doi.org/10.1029/2019GL085878

Nanometrics, 2015. Trillium Compact: User Guide. Nanometrics Inc., Kanata, Ontario, Canada, 75 pp. https://www-iuem.univ-brest.fr/pops/attachments/download/1489/trilliumcompact_userguide.pdf

Richter, C.F., 1935. An instrumental earthquake magnitude scale. *Bulletin of the Seismological Society of America*, **25**, 1-32.

Sercel, 2019. Geophones specifications. Sercel, Nantes, France. https://www.sercel.com/products/Lists/ProductSpecification/Geophones_specifications_Sercel_EN.pdf

Uhrhammer, R.A., Collins, E.R., 1990. Synthesis of Wood–Anderson seismograms from broadband digital records. *Bulletin of the Seismological Society of America*, **80**, 702–716.

Woo, J.-U., Kim, M., Sheen, D.-H., Kang, T.-S., Rhie, J., Grigoli, F., Ellsworth, W.L., Giardini, D., 2019. An in-depth seismological analysis revealing a causal link between the 2017 MW 5.5 Pohang earthquake and EGS project. *Journal of Geophysical Research, Solid Earth*, **124**, 13,060–13,078.

Supplement 3:
Magnitude correction for spectral truncation

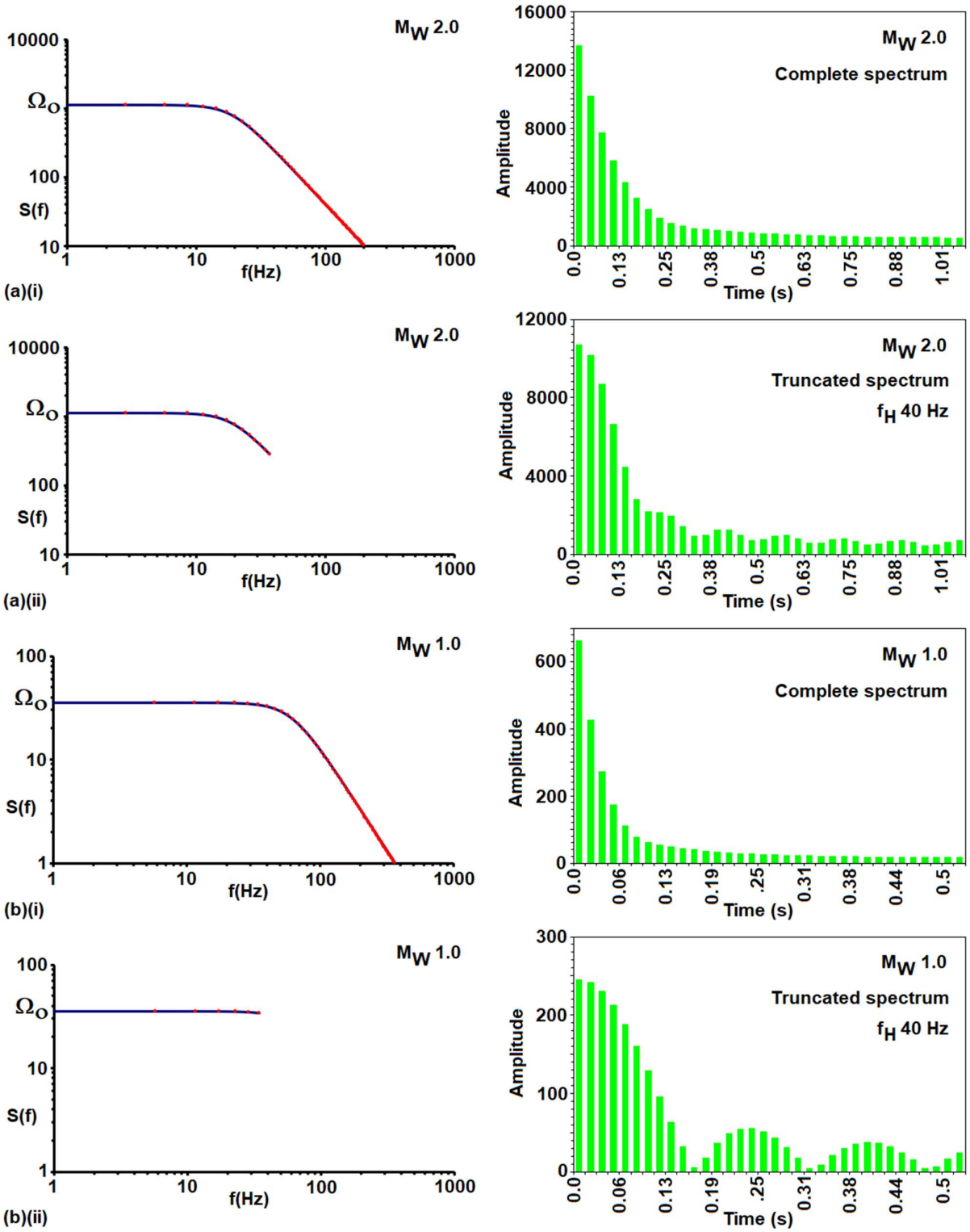

Figure S3-1. Example comparisons between example model S-wave displacement spectra, after Boatwright (1978) (equation (14) and Fig. 06), with parameter values as in Table 3, with no frequency truncation and with truncation at f_H=40 Hz, for the purpose of determining values of the parameter Ψ. **(a)** For M_W=2.0. **(b)** For M_W=1.0.

The effect of truncation of seismogram spectra, due to low recording bandwidth (i.e., low Nyquist frequency f_N), on the resulting earthquake magnitudes is investigated in order to determine a magnitude-dependent correction factor to seismogram amplitudes, Ψ, which can be used to correct the resulting magnitudes. This effect is investigated in the present study by generating 'synthetic seismograms' as inverse Fourier transforms of a coherent Brune (1970) or Boatwright (1978) model source spectrum. These have been calculated numerically, using the 'Engineers' Excel' add-on to the Excel software package (Mehta, 2006). Calculations were undertaken both with and without spectra truncated at f_H=40 Hz, the latter approximating the operational state of the digitizer at KMA station PHA2 with f_N 50 Hz and an anti-aliasing filter that cuts off circa 40 Hz. Because the phase of frequency components is not considered in this analysis, the resulting 'synthetic seismograms' are not oscillatory like real seismograms, but have well-defined amplitudes that enable the effect of spectral truncation to be assessed, the ratio of amplitudes with to without frequency truncation being designated as Ψ.

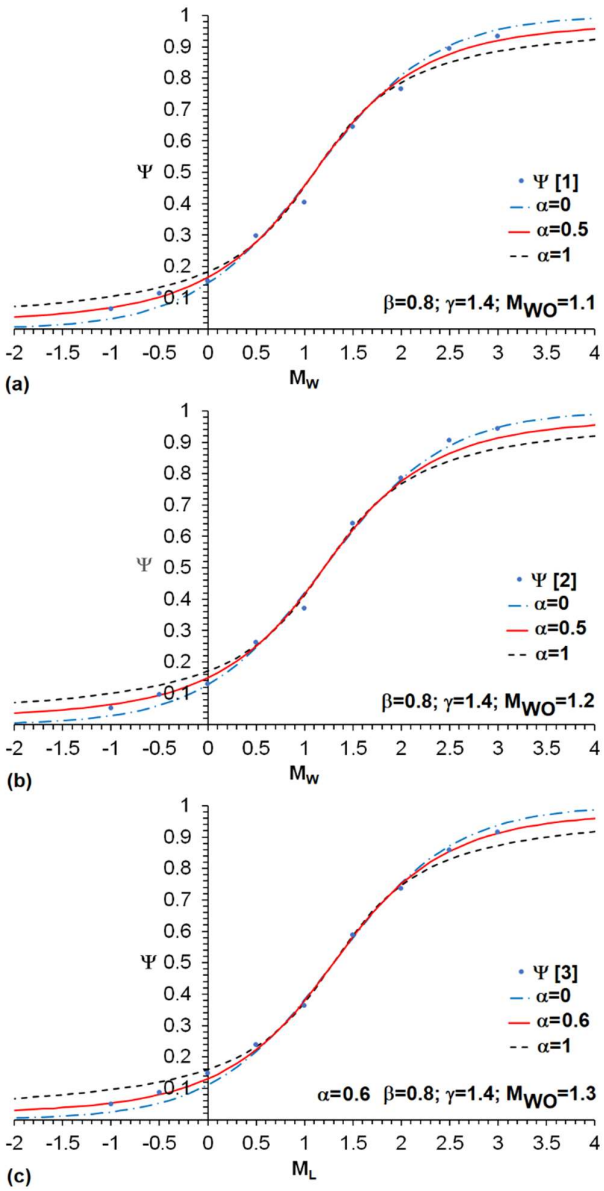

Figure S3-2. Dependence of Ψ on M_W, showing data points from Table 3 fitted using equation (S3-1) with different values (illustrated) for the parameters α, β, γ, and M_{WO}. **(a)** Curves of the form of equation (S3-1) are fitted to values of variant [1] of Ψ for a Brune (1970) source spectrum with no instrumental response. **(b)** Curves of the form of equation (S3-1) are fitted to values of variant [2] of Ψ for a Boatwright (1978) source spectrum with no instrumental response. **(c)** Curves of the form of equation (S3-1) are fitted to values of variant [3] of Ψ for a Brune (1970) source spectrum with a Wood-Anderson instrumental response.

To implement this procedure, for each value of M_W, model spectra U(f) (after Brune, 1970; equation (13)) were calculated with Ω_O in proportion to M_O and with f_C given by equation (28). The amplitudes thus calculated, without frequency truncation, were found to scale in proportion to $M_O^{1/3}$, meaning an increase by a factor of $\sqrt{10}$ for each unit increase in M_W, as expected from Boore's (1983) analysis for coherent source spectra, confirming the accuracy of this method. To assess the effect of the precise shape of the source spectrum on this analysis, the calculations were repeated for the Boatwright (1978) source spectrum in equation (14). This latter process is illustrated in Fig. 14 for the Boatwright (1978) source spectrum for representative magnitudes: M_W=2.0 (Fig. S3-1(a)), for which Ψ=0.875; and M_W=1.0 (Fig. S3-1(b)), for which Ψ=0.370. Suites of Ψ values spanning M_W 3.0 to -1.0, calculated for the same set of input parameters for both forms of the model source spectrum, are listed in Table 3.

It is evident from Table 3 that $\Psi \rightarrow 0$ at very small M_W and $\Psi \rightarrow 1$ at large M_W. A continuous empirical function that might approximate this behaviour is

$$\Psi(M_W) = \frac{\alpha}{2}\left(\tanh(\beta\,(M_W - M_{WO}) + 1\right) + \frac{(1-\alpha)}{2}\left(\frac{2}{\pi}\arctan(\gamma\,(M_W - M_{WO})) + 1\right) \qquad \text{(S3-1)}$$

where α, β, γ and M_{WO} are adjustable parameters. As Fig. S3-2(a) shows, a close fit (especially to values of Ψ for low magnitudes) for the data assuming the Brune (1970) source spectrum, but uncorrected for instrumental response, can be obtained with α=0.5, β=0.8, γ=1.4, and M_{LO}=1.1. As illustrated in Fig. S3-2(b), the results assuming the Boatwright (1978) source spectrum, again uncorrected for instrumental response, can be fitted with α=0.5, β=0.8, γ=1.4, and M_{WO}=1.2. Figure S3-2(c) shows the variation in Ψ assuming the Brune (1970) source spectrum but corrected for the instrumental response of a Wood-Anderson seismometer after Uhrhammer and Collins (1990) (Fig. S2-1(a)), fitted with α=0.6, β=0.8, γ=1.4, and M_{WO}=1.3. The lines of best fit, for α=0.5 or 0.6, in Fig. S3-2, correspond to the curves in Fig. 15.

References

Boatwright, J., 1978. Detailed spectral analysis of two small New York State earthquakes. *Bulletin of the Seismological Society of America*, **68**, 1117–1131.

Boore, D.M., 1983. Stochastic simulation of high-frequency ground motions based on seismological models of the radiated spectra. *Bulletin of the Seismological Society of America*, **73**, 1865-1894.

Brune, J., 1970. Tectonic stress and the spectra of seismic shear waves from earthquakes. *Journal of Geophysical Research*, **75**, 4997–5009 (with 1971 correction: *Journal of Geophysical Research*, **76**, 5002.

Mehta, N., 2006. Discrete Fourier Transform. Engineers Excel. http://www.engineers-excel.com/Apps/DFT/Description.htm

Uhrhammer, R.A., Collins, E.R., 1990. Synthesis of Wood–Anderson seismograms from broadband digital records. *Bulletin of the Seismological Society of America*, **80**, 702–716.

Supplement 5:
Source parameter catalogue; Explanatory notes

This supplementary file provides explanatory notes to accompany supplement 3, the spreadsheet of source parameters for earthquakes in the Pohang area. The tabs are arranged in order of reporting of results: Hofmann et al. (2019), then GSK (2019), Woo et al. (2019a), and Langenbruch et al. (2019).

Hofmann tab

Based on supplementary file 'data – seismicity' provided online by Hofmann et al. (2019), this is the definitive catalogue of source parameters for the August 2017 stimulation of well PX-1, carried out as part of the DESTRESS Horizon 2020 project. As is discussed in the main text, no source of systematic error in this set of magnitudes has been identified so no correction is necessary.

Notes:

1…Stimulation number using different notations, for comparison with other earthquake populations.

2…Date and origin time are expressed both in Universal Time (UTC) and in Korea Standard Time (KST), which is 9 hours ahead of UTC.

3…M_W and M_O were calculated in the frequency domain as discussed in the main text.

4…Peak ground velocity at seismograph station MSS01.

5…Hypocentral co-ordinates, expressed using a Cartesian co-ordinate system.

GSK_A-6 tab

Based on the initial catalogue for events near the Pohang EGS site from 2009 to the time of the 2017 Pohang mainshock, from appendix A-6 of GSK (2019). This Table includes events caused by the drilling of the sidetrack of Pohang well PX-2 into the Namsong Fault, plus events caused by the Pohang well stimulations, plus many other events that have nothing to do with the Pohang EGS project including many from the Gyeongju earthquake sequence, ~40 km south of Pohang, which began in September 2016 (e.g., Lee et al., 2018; Woo et al., 2019b).

Notes:

1…Event number allocated by GSK (2019).

2…Stimulation numbers using different notations. MS denotes the 15 November 2017 mainshock; FS denotes its foreshocks. PX2-D denotes events that occurred when drilling of the sidetrack to well PX-2 transected the Namsong Fault; GJ denotes events from the Gyeongju earthquake sequence. The 18 events labelled 'PX2-D' are from Fig. A-4-2 of GSK (2019).

3…Event reported as a template event by Woo et al. (2019a)

4…GSK (2019) Table A-6 refers to preliminary magnitude determinations for 137 events. However, these 137 magnitude determinations (40 + 59 + 38) are numerically identical, where comparisons are possible, with the 'final' determinations reported in GSK (2019) Table A-5 and by Woo et al. (2019a) and Langenbruch et al. (2020). All these magnitudes were reported by GSK (2019) as 'M_L'. For the initial 40 events they are indeed true M_L values, which appear to have been determined conventionally by synthesizing Wood-Anderson seismograms and applying the Sheen et al. (2018) distance calibration with station corrections. The next 59 magnitudes were reported as M_L by GSK (2019) but are in fact determined (as M_P) using one of the empirical prediction equations (equations (13) and (14) in the main text), and are also listed in GSK (2019) Table A-5. The remaining 38 magnitudes were also reported as M_L by GSK (2019) but are in fact likewise determined (as M_P) using one of the empirical prediction equations, but are not listed in GSK (2019) Table A-5.

5…M_W value. As discussed in the main text these values have been determined in the time domain, except for the event at 02:31:13 on 15 April 2017 and the 15 November 2017 mainshock, where frequency-domain analysis has been used.

6…M_K values, reported by KMA.

7…M_I values, reported by the EGS developer.

8…N_S denotes the number of seismograph stations with records of each event

9…This column denotes the location status of each event. 1 indicates an ambiguous candidate event with poor signal-to-noise ratio. 2 indicates an event that could not be located, so has been assigned co-ordinates for the corresponding template event. 3 indicates an event that could be located.

GSK_A-5 tab

Based on the 'definitive' catalogue for events associated with the Pohang EGS project, from appendix A-5 of GSK (2019). In addition to the 98 earthquakes listed by GSK (2019), the event at 03:58 on 31 March 2016 has been added: this is listed as one of the template events for the Pohang dataset (Woo et al., 2019a) and appears to have been omitted from this GSK (2019) table by mistake.

Notes:

1…Event number within this table, allocated by GSK (2019).

2…Corresponding event number from Table A-6, allocated by GSK (2019).

3…Stimulation numbers using different notations. MS denotes the 15 November 2017 mainshock; FS denotes its foreshocks. PX2-D denotes an event that occurred when drilling of the sidetrack to well PX-2 transected the Namsong Fault.

4…This column denotes the location status of each event, after Table A-6. For all events listed here, this is 3, indicating an event that could be located, rather than one assigned the nominal co-ordinates of a corresponding template event.

5…Template event used in template matching. These were not reported by GSK (2019) but the set of events used was listed by Woo et al. (2019a). For some reason, the event at 03:58 on 31 March 2016 was omitted by GSK (2019) from this table.

6…M_L value from GSK (2019). These values appear to have been determined conventionally by synthesizing Wood-Anderson seismograms and applying the Sheen et al. (2018) distance calibration with station corrections. M_L for the 15 November 2017 mainshock was also determined using this method by this was not used as a template event because its large size precluded waveform matching with smaller events.

7…Magnitude reported as M_L by GSK (2019) but in fact determined (as M_P) using one of the empirical prediction equations (equations (13) and (14) in the main text).

8…M_W value, from GSK (2019). As discussed in the main text these values have been determined in the time domain, except for the event at 02:31:13 on 15 April 2017 and the 15 November 2017 mainshock, where frequency-domain analysis has been used.

9…M_K values, reported by KMA for events with $M_K \geq 2.0$.

10…M_W values, from GSK (2019), after correction as explained in the main text, as displayed in Fig. 12(a).

11…M_L values, from GSK (2019), after correction with $\delta M_L=1.2$ as explained in the main text, as displayed in Fig. 14(a).

12…M_L values, from GSK (2019), after correction with $\delta M_L=0$ as explained in the main text, as displayed in Fig. 14(c).

13…The totals all include the event at 03:58 on 31 March 2016 so are all one greater than the corresponding totals reported by GSK (2019).

GSK_Stn_Corr tab

Based on Fig. 5-7 of GSK (2019), which is reproduced here in different formats as Fig. #S1-2 of supplement 1 and Fig. 9 in the main text.

Notes:

1…Station network according to GSK (2019). Except for the stations of the permanent KMA and KIGAM networks, the designations used provide no information regarding which organization was responsible for each station.

2…Type of station, where identified by GSK (2019): Acc., accelerometer; B.Acc., borehole accelerometer; BB, broadband; SP, and short period.

3…Inferred seismograph station for which the station correction is reported by GSK (2019), where possible, based on the station codes illustrated in Fig. 5-1 of GSK (2019), which is reproduced here in different formats as Fig. #S1-1 of supplement 1 and Fig. 3 in the main text.

4…Inferred possible alternative station type, based on Fig. 5-1 of GSK (2019), reproduced here in different formats as Fig. #S1-1 of supplement 1 and Fig. 3 in the main text.

5…Station correction, S, ± one standard deviation (S.D. (S)), digitized from Fig. 5-1 of GSK (2019).

Woo_Templates tab

Based on supplementary Table S2 of Woo et al. (2019a), this is the catalogue of source parameters for the set of template events used by Woo et al. (2019a) (and by GSK, 2019), for their matched filter analysis.

Notes:

1…Stimulation numbers using different notations. MS denotes the 15 November 2017 mainshock; FS denotes its foreshocks. PX2-D denotes an event that occurred when drilling of the sidetrack to well PX-2 transected the Namsong Fault.

2…M_L values determined using the Sheen et al. (2018) formula. These are the same set of values as were reported by GSK (2019) but rounded to two decimal places instead of three.

Woo_Catalogue tab

Based on supplementary catalogue 2 of Woo et al. (2019a), this is the catalogue of source parameters for the set of relocated events reported by Woo et al. (2019a). All the information presented by these authors was taken from GSK (2019), something they did not mention.

Notes:

1…Event number allocated by Woo et al. (2019a).

2…Stimulation numbers using different notations. MS denotes the 15 November 2017 mainshock; FS denotes its foreshocks. PX2-D denotes an event that occurred when drilling of the sidetrack to well PX-2 transected the Namsong Fault.

3…Hypocentral co-ordinates reported 'after relocation'. For all events these are the same as for GSK (2019).

4…T denotes events adopted as template events. For some reason the event at 03:58 on 31 March 2016, recognised as a template event in the list of these events (see above), was omitted by Woo et al. (2019), apparently by mistake.

5…M_L value, reported as original but in fact from GSK (2019). These values appear to have been determined conventionally by synthesizing Wood-Anderson seismograms and applying the Sheen et al. (2018) distance calibration with station corrections after GSK (2019). M_L for the 15 November 2017 mainshock was also determined using this method by this was not used as a template event because its large size precluded waveform matching with smaller events.

6…Value reported by Woo et al. (2019a) as M_L but in fact M_P obtained (as for GSK, 2019) using one or other of the empirical prediction equations.

7…M_W value, reported as original but in fact from GSK (2019). As discussed in the main text these values have been determined in the time domain, except for the event at 02:31:13 on 15 April 2017 and the 15 November 2017 mainshock where frequency-domain analysis has been used. M_W for the event at 03:58 on 31 March 2016, omitted by Woo et al. (2019a), apparently by mistake, is from GSK (2019).

8…M_K values, reported by KMA for events with $M_K \geq 2.0$.

9…M_I values, reported by the EGS developer.

10…M_P values, from GSK (2019), after correction as explained in the main text, as displayed in Fig. 13(a).

11…The totals all include the event at 03:58 on 31 March 2016 so are all one greater than the corresponding totals reported by Woo et al. (2019a).

Langenbruch tab

This is based on the catalogue of earthquake source parameters posted online by Langenbruch et al. (2020) at https://zenodo.org/record/3596374#.X3x9me17nIU

Notes:

1…Event number allocated by Langenbruch et al. (2020).

2…Stimulation numbers using different notations. MS denotes the 15 November 2017 mainshock; FS denotes its foreshocks.

3…T denotes events adopted as template events.

4…Existing M_L value from GSK (2019) and Woo et al. (2019a). These values appear to have been determined conventionally by synthesizing Wood-Anderson seismograms and applying the Sheen et al. (2018) distance calibration.

5…Existing M_P value from GSK (2019) and Woo et al. (2019a), reported by Langenbruch et al. (2020) as M_L.

6…Value reported by Langenbruch et al. (2020) as M_L, but in fact a M_P value listed in Table A-6 of GSK (2019).

7… Value reported by Langenbruch et al. (2020) as M_L, which had not been reported previously. From the wording of the online supplement to by Langenbruch et al. (2020), these values are inferred to be M_P determined using one of the empirical prediction equations.
8…Magnitude M_T reported by Langenbruch et al. (2020) as determined by template matching, using one of the template events indicated, although the template event used for each determination is not specified.
9…Values reported by Langenbruch et al. (2020) as M_T but which are in fact M_L values from template events, repeated. This is not immediately obvious because when presented as 'M_T' values they are rounded to two decimal places instead of three.
10…Magnitude M_T reported by Langenbruch et al. (2020) for events caused by stimulations of well PX-2, as determined by template matching, after correction using equation (18) with M_R=2.0 and $\Gamma=1/\log_{10}(20)\approx0.769$, as displayed in Fig. 16(a). Events with magnitude ≥M_R=2.0 (highlighted) are unaffected by this correction. Note that, below this threshold, the correction procedure has been applied to magnitudes of template events as well as to magnitudes obtained by template matching.
11…Magnitude M_T reported by Langenbruch et al. (2020) for events caused by stimulations of well PX-2, as determined by template matching, after correction using equation (18) with M_R=2.0 and Γ=0.64, as displayed in Fig. 16(b). Events with magnitude ≥M_R=2.0 (highlighted) are unaffected by this correction. Note that, below this threshold, the correction procedure has been applied to magnitudes of template events as well as to magnitudes obtained by template matching.
12…Magnitude M_T reported by Langenbruch et al. (2020) for other events, as determined by template matching, after correction using equation (18) with M_R=2.0 and $\Gamma=1/\log_{10}(20)\approx0.769$. Events with magnitude ≥M_R=2.0 (highlighted) are unaffected by this correction. Note that, below this threshold, the correction procedure has been applied to magnitudes of template events as well as to magnitudes obtained by template matching.
13…Magnitude M_T reported by Langenbruch et al. (2020) for other events, as determined by template matching, after correction using equation (18) with M_R=2.0 and Γ=0.64. Events with magnitude ≥M_R=2.0 (highlighted) are unaffected by this correction. Note that, below this threshold, the correction procedure has been applied to magnitudes of template events as well as to magnitudes obtained by template matching.
14…Corrected M_L value for δM_L=0 from the GSK_A-5 tab.
15…Corrected M_L value for δM_L=1.2 from the GSK_A-5 tab.
14…Corrected M_W value from the GSK_A-5 tab.

References

GSK, 2019. Final Report of the Korean Government Commission on relations between the 2017 Pohang Earthquake and EGS Project. The Geological Society of Korea, Seoul, 427 pp. (in Korean). https://data.doi.or.kr/10.22719/KETEP-2019043001

Hofmann, H., Zimmermann, G., Farkas, M., Huenges, E., Zang, A., Leonhardt, M., Kwiatek, G., Martinez-Garzon, P., Bohnhoff, M., Min, K.-B., Fokker, P., Westaway, R., Bethmann, F., Meier, P., Yoon, K.S., Choi, J.W., Lee, T.J., Kim, K.Y., 2019. First field application of cyclic soft stimulation at the Pohang Enhanced Geothermal System site in Korea. *Geophysical Journal International*, **217**, 926–949.

Langenbruch, C., Ellsworth, W.L., Woo, J.-U., Wald, D.J., 2020. Value at induced risk: injection-induced seismic risk from low-probability, high-impact events. *Geophysical Research Letters*, **47**, e2019GL085878, 12 pp., https://doi.org/10.1029/2019GL085878

Lee JiMin, Ryoo YongGyu, Park Sun Cheon, Ham Young Mo, Park Jong Soo, Kim Myeong Su, Park Sang Mi, Cho Hyen Geom, Lee Keun Su, Kim In Sun, Kim Hye Su, Bae SunHee, 2018. Seismicity of the 2016 M_L 5.8 Gyeongju earthquake and aftershocks in South Korea. *Geosciences Journal*, **22**, 433–444.

Sheen Dong-Hoon, Kang Tae-Seob, Rhie JunKee, 2018. A local magnitude scale for South Korea. *Bulletin of the Seismological Society of America*, **108**, 2748–2755.

Woo Jeong-Ung, Kim, M., Sheen, D.-H., Kang, T.-S., Rhie, J., Grigoli, F., Ellsworth, W.L., Giardini, D., 2019a. An in-depth seismological analysis revealing a causal link between the 2017 M_W 5.5 Pohang earthquake and EGS project. *Journal of Geophysical Research, Solid Earth*, **124**, 13,060–13,078.

Woo Jeong-Ung, Rhie JunKee, Kim SeongRyong, Kang Tae-Seob, Kim Kwang-Hee, Kim YoungHee, 2019b. The 2016 Gyeongju earthquake sequence revisited: aftershock interactions within a complex fault system. *Geophysical Journal International*, **217**, 58–74.